

Article

Preparation of Mesoporous and/or Macroporous SnO₂-Based Powders and Their Gas-Sensing Properties as Thick Film Sensors

Luyang Yuan ¹, Takeo Hyodo ², Yasuhiro Shimizu ^{2,*} and Makoto Egashira ²

¹ Graduate School of Science and Technology, Nagasaki University, 1-14 Bunkyo-machi, Nagasaki 852-8521, Japan; E-Mail: d708057c@cc.nagasaki-u.ac.jp (L.Y.)

² Faculty of Engineering, Nagasaki University, 1-14 Bunkyo-machi, Nagasaki 852-8521, Japan; E-Mails: hyodo@nagasaki-u.ac.jp (T.H.); egashira@nagasaki-u.ac.jp (M.E.)

* Author to whom correspondence should be addressed; E-Mail: shimizu@nagasaki-u.ac.jp; Tel.: +81-95-819-2642; Fax: +81-95-819-2643.

Received: 13 December 2010 / in revised form: 10 January 2011 / Accepted: 19 January 2011 /

Published: 25 January 2011

Abstract: Mesoporous and/or macroporous SnO₂-based powders have been prepared and their gas-sensing properties as thick film sensors towards H₂ and NO₂ have been investigated. The mesopores and macropores of various SnO₂-based powders were controlled by self-assembly of sodium bis(2-ethylhexyl)sulfosuccinate and polymethyl-methacrylate (PMMA) microspheres (*ca.* 800 nm in diameter), respectively. The introduction of mesopores and macropores into SnO₂-based sensors increased their sensor resistance in air significantly. The additions of SiO₂ and Sb₂O₅ into mesoporous and/or macroporous SnO₂ were found to improve the sensing properties of the sensors. The addition of SiO₂ into mesoporous and/or macroporous SnO₂ was found to increase the sensor resistance in air, whereas doping of Sb₂O₅ into mesoporous and/or macroporous SnO₂ was found to markedly reduce the sensor resistance in air, and to increase the response to 1,000 ppm H₂ as well as 1 ppm NO₂ in air. Among all the sensors tested, meso-macroporous SnO₂ added with 1 wt% SiO₂ and 5 wt% Sb₂O₅, which were prepared with the above two templates simultaneously, exhibited the largest H₂ and NO₂ responses.

Keywords: mesopore; macropore; meso-macropore; SnO₂ gas sensors; SiO₂; Sb₂O₅

1. Introduction

In recent years, the development for porous materials is been an essential objective of materials science research. This interest is the result of the progress in all fields of industry and technology [1-5]. According to the IUPAC definition, microporous materials are those with pore diameters less than 2 nm, mesoporous materials are those that have pore diameters between 2 and 50 nm, and macroporous materials are those with pores bigger than 50 nm [6]. Among them, macroporous and mesoporous silica with sufficient thermal stability has been applied to catalysts [7,8] membranes [9], adsorbents [10], chemical sensors [11] and templates for nanowires [12]. On the contrary, the poor thermal stability of non-silica mesoporous materials limits their applications. Over the past 50 years, semiconductor metal oxides such as SnO_2 , ZnO and In_2O_3 have been extensively studied as gas sensing materials due to their various advantages such as the facile fabrication process of thin and thick films, low cost and high thermal stability [13,14]. Among the various metal oxides, SnO_2 is one of the most attractive materials for semiconductor gas sensors [13-23] operated at elevated temperatures (200–600 °C). The gas sensing property of semiconductor gas sensors is largely dependent on various factors such as shape and size of the oxide particles [24-30]. In addition, strict control of nanostructure of the oxide powders is also quite effective in improving the gas sensing properties [31-34]. Thus, our group's efforts have so far been directed to preparing thermally stable mesoporous (m-) [15-17] and macroporous (mp-) [18,21] oxide films. However, the H_2 sensing properties of the m- SnO_2 sensors were relatively lower than expected from their large specific surface area and mp- SnO_2 showed rather excellent sensing properties to H_2 . Moreover, our recent studies have demonstrated the successful preparation of thermally stable meso-macroporous (m mp-) SnO_2 and the improvement of gas sensing properties by employing pellet-type sensor structures [19]. However, the mechanical strength of the m mp- SnO_2 pellets was not enough for long-term operation and this then became a subject for further investigation.

The present study is thus directed to developing m-, mp- and m mp- SnO_2 thick film sensors. The sensors were fabricated by screen-printing of their as-prepared powders, which were produced by employing sodium bis(2-ethylhexyl)sulfosuccinate (aerosol-OT, AOT) as a mesopore template and PMMA microspheres with an average diameter of 800 nm as a macropore template, and then subsequent calcination at 600 °C for 5 h. The effects of the addition of SiO_2 and Sb_2O_5 to m-, mp- and m mp- SnO_2 powders on their H_2 and NO_2 sensing properties were also examined.

2. Experimental Section

2.1. Preparation of Mesoporous and/or Macroporous SnO_2 -Based Powders

Various SnO_2 -based powders with well-developed mesopores and/or macropores were prepared by a sol-gel method using $\text{SnCl}_4 \cdot 5\text{H}_2\text{O}$ (Kishida Chem. Co., Ltd.) as a Sn source, AOT (Kishida Chem. Co., Ltd.) as a mesopore template and PMMA microspheres with an average diameter of 800 nm (MP-1600, Soken Chem. & Eng. Co., Ltd.) as a macropore template. A given amount of $\text{SnCl}_4 \cdot 5\text{H}_2\text{O}$ (1.75 g) was mixed in 400 mL of ultra pure water together with an appropriate amount of AOT and/or PMMA microspheres. In some cases, appropriate amounts of tetraethoxysilane (TEOS, Kishida Chem. Co., Ltd.) and/or SbCl_3 (Kishida Chem. Co., Ltd.) were also added to the solution, in

order to prepare SnO₂ powders added with the given amounts of SiO₂ and/or Sb₂O₅. Then the pH value of the resulting mixture was adjusted to 8.5 by adding an aqueous solution of NH₃. The solid product obtained was aged in the solution at 20 °C for 3 days, then the resulting product was separated from the solution by centrifugation. After drying the product in an oven at 80 °C overnight, the resulting powder product was treated with a 0.1 mol L⁻¹ phosphoric acid solution for about 2 h, and the resulting product was dried in an oven at 80 °C overnight. The powder product resulting after pulverization is referred to as-prepared powder. The as-prepared powders were used for fabricating thick film sensors, but for the characterization tests, as-prepared powders were subjected to calcination at 600 °C for 5 h in air, which are the same conditions adopted for the thick film sensors after the screen-printing of a paste of as-prepared powders. The preparation conditions and compositions of all SnO₂-based powders obtained in this study and their abbreviations are summarized in Table 1.

Table 1. Preparation conditions of SnO₂-based powders.

Sensors		Mesopore template (AOT) /g*	Macropore template (PMMA) /g*	Amount of MO added to SnO ₂ (x or y)/wt%	
Kind of powder	Abbreviation			MO: Sb ₂ O ₅ (using NbCl ₅)	MO: SiO ₂ (using TEOS)
Mesoporous (m-) SnO₂	m-T0S0	1.75	none	none	none
	m-T1S0			5.0	1.0
	m-T1S5			5.0	1.0
Meso- macroporous (m·mp-) SnO₂	m·mp-T1S0	1.75	0.35	none	
	m·mp-T1S0.5			0.5	
	m·mp-T1S1			1.0	1.0
	m·mp-T1S3			3.0	
	m·mp-T1S5			5.0	
Macroporous (mp-) SnO₂	mp-T1S0	none	0.35	none	
	mp-T1S0.5			0.5	
	mp-T1S1			1.0	1.0
	mp-T1S3			3.0	
	mp-T1S5			5.0	

* In 400 mL aqueous solution.

In our study, the SnO₂-based powders prepared using AOT or PMMA microspheres as a template are identified by using abbreviations such as m-TxSy or mp-TxSy, respectively, and the SnO₂-based powder prepared using both AOT and PMMA microspheres as templates is indicated as m mp-TxSy, as shown in Table 1. Here, T and S mean the addition of TEOS and SbCl₃ in the precursor solution, respectively, and *x* (*x* = 0, 1, 5) and *y* (*y* = 0, 1, 5) represent the added amounts of SiO₂ and Sb₂O₅ (wt%) with respect to the weight of SnO₂, respectively, on the basis of the expected weight of constituent oxides after calcination.

Crystal phase and crystallite size of SnO₂-based powders were characterized with X-ray diffraction (XRD, CuKα, Shimadzu Corp., RINT-2200). The crystallite size was calculated by using Scherrer's formula:

$$CS = 0.89\lambda/\beta\cos\theta \quad (1)$$

where λ is the wavelength of $\text{CuK}\alpha$, β is the full-width at the half-maximum of the (110) line and θ is the diffraction angle of the (110) peak. The specific surface area, pore volume and pore size distribution of SnO_2 -based powders were measured by the BET method using a N_2 sorption isotherm (Micromeritics Instrument Corp., TriStar3000). Morphology of SnO_2 -based thick films was observed by a scanning electron microscope (SEM, JEOL Ltd., JCM-5700).

2.2. Fabrication of Mesoporous and/or Macroporous SnO_2 -Based Thick Film Sensors

The as-prepared SnO_2 -based powder was mixed with a printing oil which is composed of an alkyl ester of methacrylic acid as a binder, a toluene-based solvent, and an ammonium salt of polyacrylic acid as a plasticizer, and the resulting paste was screen printed on an alumina substrate, on which a pair of interdigitated Pt electrodes (gap between electrodes: 130 μm) had been printed (the thickness of the film was controlled to be about 20 μm after calcination for all the sensors fabricated). Then the printed film was subjected to heat treatment at 600 $^\circ\text{C}$ for 5 h in air prior to response measurements. The gas-sensing properties of the thick film sensors to 1,000 ppm H_2 and 1 ppm NO_2 balanced with air were measured in the temperature range of 350–500 $^\circ\text{C}$. The magnitude of the gas response was defined as the ratio (R_a/R_g) of the sensor resistance in air (R_a) to that in a target gas (R_g) for H_2 , but the reverse ratio (R_g/R_a) was used for NO_2 .

3. Results and Discussion

3.1. Characterization of Mesoporous and/or Macroporous SnO_2 -Based Powders

Pore size distribution and specific surface area (SSA) of representative m- SnO_2 , mp- SnO_2 and m mp- SnO_2 powders after calcination are shown in Figure 1. As shown in Figures 1(a-i), m-T0S0 powder, which was prepared only with the addition of AOT, showed a SSA of 150.9 $\text{m}^2 \text{g}^{-1}$ and a larger pore volume of 0.153 $\text{cm}^3 \text{g}^{-1}$ with a pore diameter of ca. 3.1 nm at the maximum pore volume (hereafter, it will be referred to as the maximum pore diameter). The characterization data of representative SnO_2 -based powders is summarized in Table 2. The addition of 1 wt% SiO_2 to m-T0S0 induced a slight increase in SSA (162.3 $\text{m}^2 \text{g}^{-1}$) and reduced the maximum pore diameter to ca. 2.7 nm (see m-T1S0). This result implies the repression of growth of SnO_2 crystallites and/or grains by the added SiO_2 , as was reported by Fukuoka *et al.* [12]. Simultaneous addition of 1 wt% SiO_2 and 5 wt% Sb_2O_5 to m-T0S0 resulted in further increase in SSA slightly to a value of 176.5 $\text{m}^2 \text{g}^{-1}$ (see m-T1S5). Thus, the addition of Sb_2O_5 was suggested to be also effective in controlling grain growth, which will be confirmed by the change in SnO_2 crystallite size discussed later.

It was revealed that the introduction of macropores into m-T1S5 was very effective for increasing SSA to a value of 262.7 $\text{m}^2 \text{g}^{-1}$ (see m mp-T1S5, Figures 1(c-ii)). This arises undoubtedly from the decrease in the maximum pore diameter and the increase in pore volume, as summarized in Table 2. On the other hand, the introduction of macropores only (mp-T1S5), instead of mesopores (m-T1S5), into SnO_2 -based powder reduced SSA to a value of 112.0 $\text{m}^2 \text{g}^{-1}$ (compare Figure 2(b-ii) with Figure 2(a-iii)) and then decreased pore volume (see Table 2). From these results, it is confirmed that the introduction of mesopores is essential for obtaining both large specific surface and large pore volume of SnO_2 -based powders.

Figure 1. Pore size distributions and specific surface area of representative (a) m-SnO₂, (b) mp-SnO₂ and (c) m·mp-SnO₂ powders.

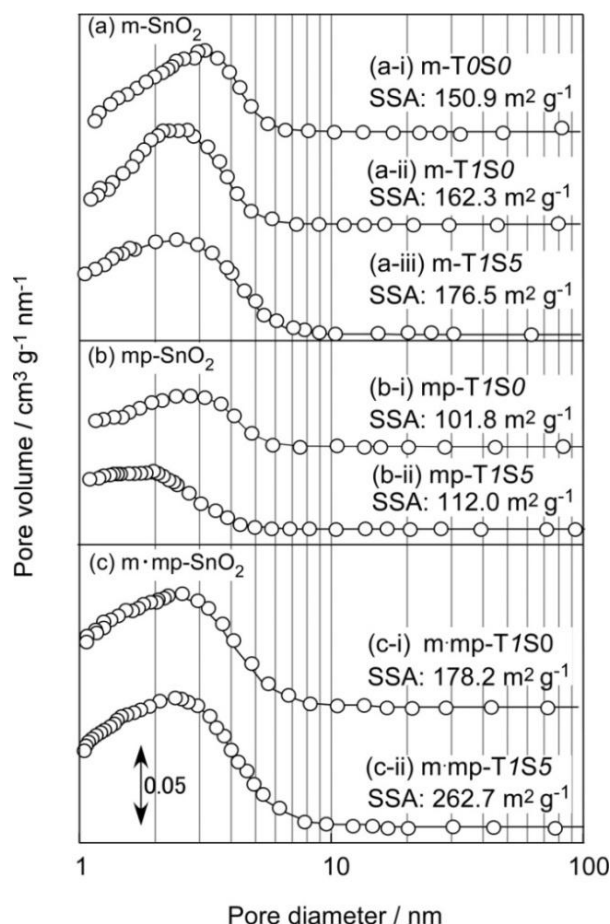


Table 2. Characterization data of representative m-SnO₂, mp-SnO₂ and m·mp-SnO₂ powders.

Sensors		Specific surface	Pore	Maximum pore	Crystallite size
Kind of powder	Abbreviation	area (SSA) /m ² g ⁻¹	volume /cm ³ g ⁻¹	diameter * /nm	(CS) /nm
m-SnO ₂	m-T0S0	150.9	0.153	3.1	7.0
	m-T1S0	162.3	0.160	2.7	3.8
	m-T1S5	176.5	0.155	2.5	3.2
m·mp-SnO ₂	m·mp-T1S0	178.2	0.184	2.5	4.2
	m·mp-T1S5	262.7	0.191	2.3	3.2
mp-SnO ₂	mp-T1S0	101.8	0.090	2.9	3.9
	mp-T1S5	112.0	0.079	2.0	2.7

* Pore diameter at the maximum pore volume in the pore size distribution curve.

Figure 2 shows variations in SSA of representative SnO₂-based powders with amount of Sb₂O₅ added. The effect of the Sb₂O₅ on SSA can be seen more clearly from this figure. As for the cases of m-T1Sy and mp-T1Sy series, SSA values increased slightly with increasing amounts of Sb₂O₅ added, but only for the m·mp-T1Sy series, it is obvious that SSA increased markedly with an increase in the additive amount of Sb₂O₅ reaching the largest value of 262.7 m² g⁻¹ obtained in the present study. The

reason for this preferable effect for sensor application observed only the m mp-T/Sy series is not yet clarified and is a subject for future work.

Figure 2. Variations in specific surface area of representative SnO₂-based powders with amounts of Sb₂O₅ added.

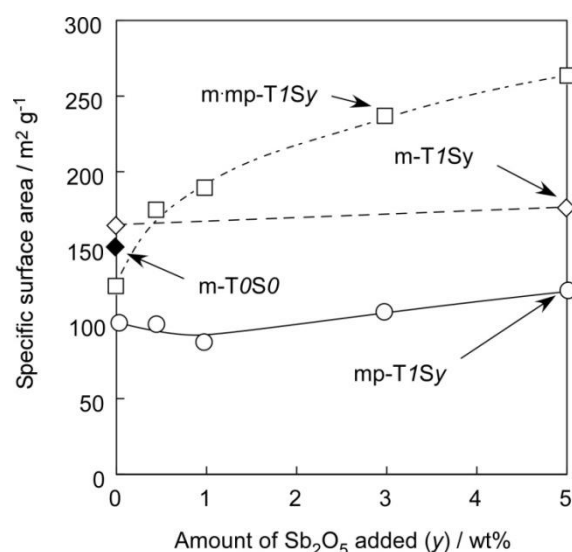
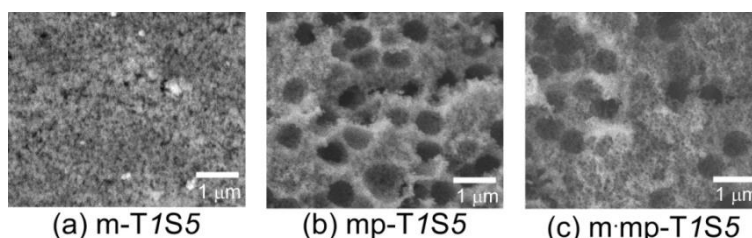


Figure 3 shows the SEM images of the fracture surface of m-T/S5, mp-T/S5 and m mp-T/S5 thick film sensors. No formation of macropores in m-T/S5 is reasonable, since no PMMA microspheres were added, as shown in Figure 3(a). But, Figure 3(b,c) confirm the formation of many spherical macropores originating from the morphology of PMMA microspheres as a template in the mp-T/S5 and m mp-T/S5 thick film sensors. However, the diameter of macropores observed was in the 400–750 nm range, which was smaller than that of the diameter of raw PMMA microspheres, due to shrinkage of resulting voids during the growth of SnO₂ crystallites.

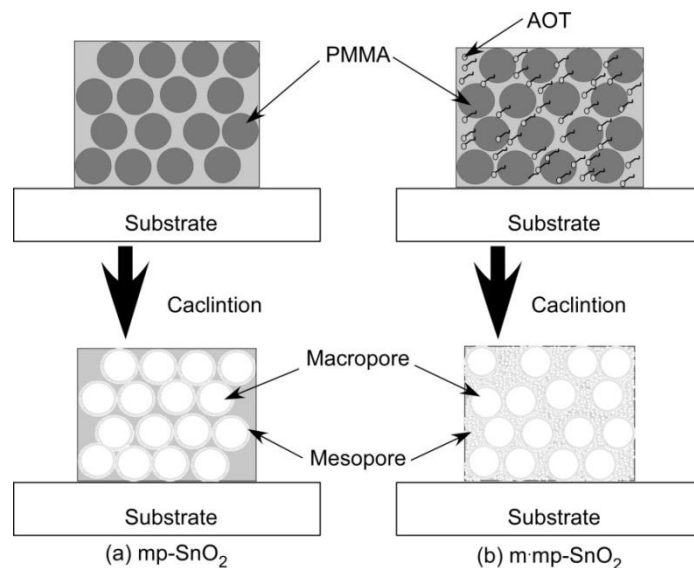
Figure 3. SEM images of fracture surface of (a) m-T/S5, (b) mp-T/S5 and (c) m mp-T/S5 thick film sensors.



As shown in Figure 1 and Table 1, mp-SnO₂ powder prepared in the present study showed relatively larger SSA than the conventional SnO₂ powder (8.4 m² g⁻¹, [35]), indicating the formation of a certain amount of mesopores, irrespective of the addition or not of AOT as a mesoporous structure template. This result implies penetration or diffusion of PMMA fragments into the dried SnO₂ precursor material during the calcination and such fragments may act as a mesoporous template at the interface between the PMMA microsphere and surrounding dried SnO₂ precursor. Thus, after the calcination at 600 °C for 5 h of the mp-SnO₂ thick film, a thin mesoporous layer may be formed at the interface between the

pores and SnO_2 particles, as shown schematically in Figure 4(a) [36]. As for m mp- SnO_2 , it is considered that mesopores are formed uniformly inside all the SnO_2 particles and the whole thick film structure, as shown in Figure 4(b).

Figure 4. Schematic drawing of formation mechanism of mesopores and macropores in (a) mp- SnO_2 and (b) m mp- SnO_2 thick film sensors.



Another notable finding in Figure 3 is a relatively longer distance of the macropores in m mp-T/S5 than that in mp-T/S5. Since AOT was used as a mesoporous template in fabricating m mp- SnO_2 powder, thermal decomposition and subsequent firing along with generation of combustion gases may induce sponge and/or bulky structure with mesopores, leading to a longer distance of the macropores, as also shown schematically in Figure 4(b).

Figure 5 shows XRD patterns of representative m- SnO_2 , mp- SnO_2 and m mp- SnO_2 powders. Diffraction peaks of all powders were rather broad, indicating low crystallinity, but all peaks could be ascribed to those of tetragonal SnO_2 . The CS value which was calculated for each powder using Scherrer's formula is summarized in Table 2. Variations in CS of representative SnO_2 -based powders are shown Figure 6. On the whole, the CS values were small and were in a range of 2.7–7 nm in diameter, due to the limitation of crystallite growth induced by the phosphoric acid treatment before the calcination [15,16]. Exceptionally, m-T/S0 showed the largest CS value of 7 nm. The CS value was decreased drastically to 3.8 nm by the addition of 1 wt% SiO_2 to m-T/S0 (see m-T/S1 in Table 2 and Figure 6). Thus, the repression of the growth of SnO_2 crystallites by the added SiO_2 could be confirmed from these results [37]. As for the powders containing 1 wt% SiO_2 , CS values were almost comparable, whereas they tended to decrease slightly with increasing amounts of the Sb_2O_5 additive in each series. In addition, the kind of porous structure, *i.e.*, mesopore, macropore, and mesopore plus macropore, was found to have only a little effect on controlling the CS values. Thus, we can confirm again that the addition of 1 wt% SiO_2 was the most powerful method in reducing the CS value among several factors. The CS values decreased slightly by the Sb_2O_5 addition in each series, but no diffraction peaks other than SnO_2 were observed in XRD patterns even for the cases of 5 wt% Sb_2O_5 addition (Figure 5). This implies that Sb ions added were sufficiently incorporated into the SnO_2

crystal lattice and this solid-solution is also effective for the repression of the crystal growth among SnO_2 -based crystallites [23,38,39]. These results demonstrate that the pore size distribution, SSA and CS values of SnO_2 -based powders can be controlled by selecting the kinds of templates, the kind of additives and their additive amounts.

Figure 5. XRD patterns of (a) m- SnO_2 , (b) mp- SnO_2 and (c) m mp- SnO_2 powders.

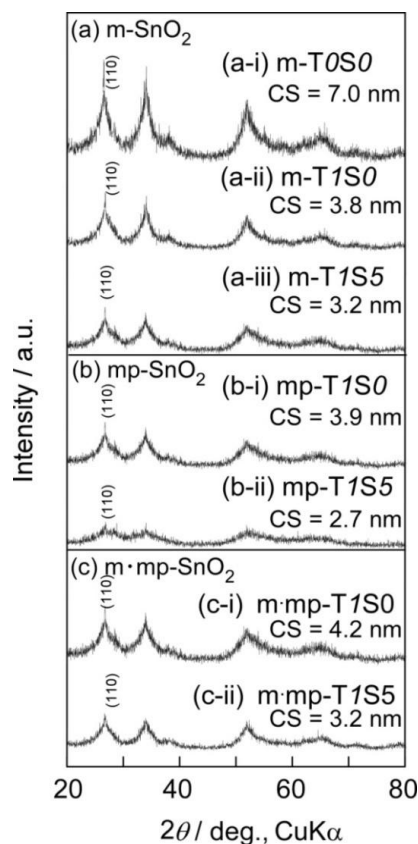
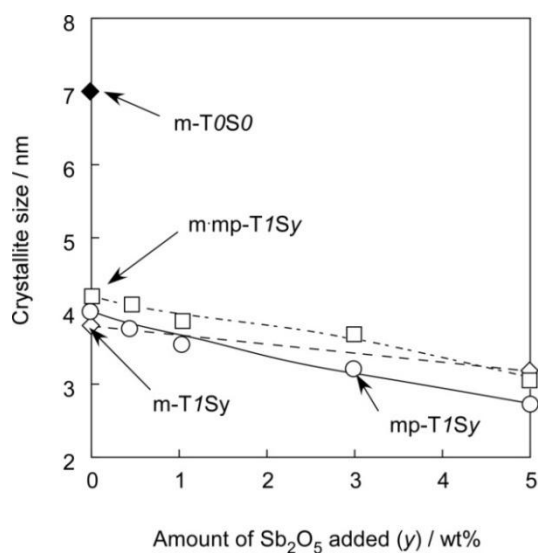


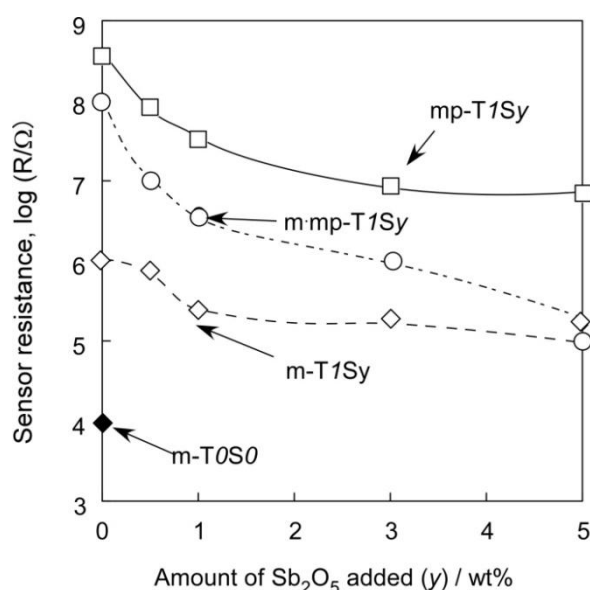
Figure 6. Variations in crystallite size of representative SnO_2 -based powders with amounts of Sb_2O_5 added.



3.2. H_2 and NO_2 Sensing Properties of Mesoporous and/or Macroporous SnO_2 -Based Sensors

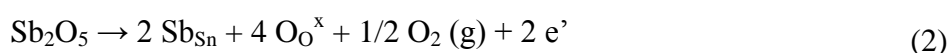
Variations in sensor resistance of SnO_2 -based thick film sensors in air at 450 °C with amounts of Sb_2O_5 added are shown in Figure 7. The m-T0S0 sensor showed the lowest resistance in air, but the addition of 1 wt% SiO_2 to m-T0S0 increased the sensor resistance in air (see m-T1S0). The sensor resistance of other two series sensors, *i.e.*, mp-T1S0 and m mp-T1S0, in air was also very high. Even if Si^{4+} ions would be substituted for Sn^{4+} ion sites, no valency control effect could be expected. Therefore, SiO_2 added was anticipated to be segregated among SnO_2 crystallites and/or grains and then to reduce electronic conduction of SnO_2 -based thick film sensors, although the segregation of SiO_2 was not confirmed by the XRD measurements due to its small amount added.

Figure 7. Variations in sensor resistance of SnO_2 -based thick film sensors in air at 450 °C with amounts of Sb_2O_5 added.



Introduction of macropores into SnO_2 by using PMMA microspheres (see mp-T1S0 series), instead of the introduction of mesopores, and/or the simultaneous introduction of macropores (see m mp-T1S0 series) also resulted in an increase in sensor resistance. This phenomenon can be considered to arise mainly from the introduction of air voids, which are electrical insulators, via various pores in the thick film sensors, but the mp-T1S0 sensor with macropores showed the largest resistance in air, irrespective of the smallest pore volume, among three series of sensors. This fact implies the existence of another factor, besides the pore volume, in determining the sensor resistance in air, such as the manner of distribution of pores in the thick film and so on, though the details are not clear at present.

In each sensor series, the sensor resistance in air decreased with increasing amounts of Sb_2O_5 additive. This behavior can be explained by the valency control, *i.e.*, partial substitution of Sn^{4+} sites with Sb^{5+} ions, producing free electrons, as described in Equation (2) [38–40]:



These results also confirm the existence of substituted Sb^{5+} ions, *i.e.*, the solid-solution of between Sb_2O_5 and SnO_2 and then little amount of segregated Sb_2O_5 among SnO_2 -based particles.

Figures 8 and 9 show temperature dependence of response of SnO₂-based thick film sensors to 1,000 ppm H₂ balanced with air and 1 ppm NO₂ balanced with air. Almost all sensors showed the maximum response to 1,000 ppm H₂ at a temperature of 450 °C. In contrast, the response to 1 ppm NO₂ of all sensors tended to increase as the operating temperature decreased, and showed the largest response in the temperature range studied at 350 °C.

Figure 8. Temperature dependence of response SnO₂-based thick film sensors to 1,000 ppm H₂.

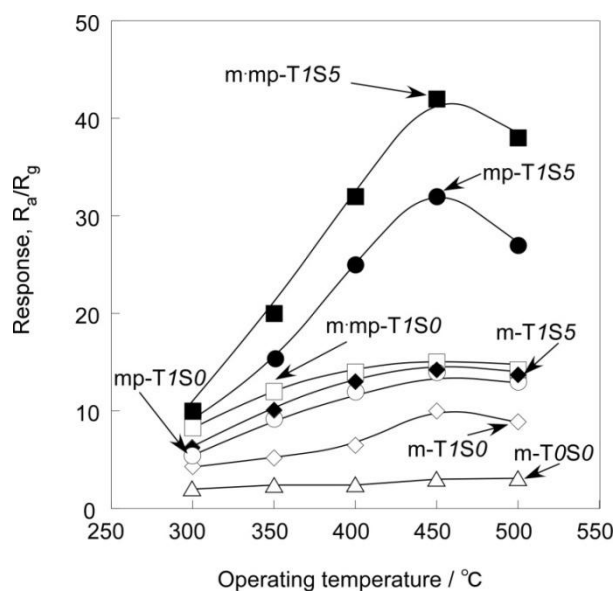
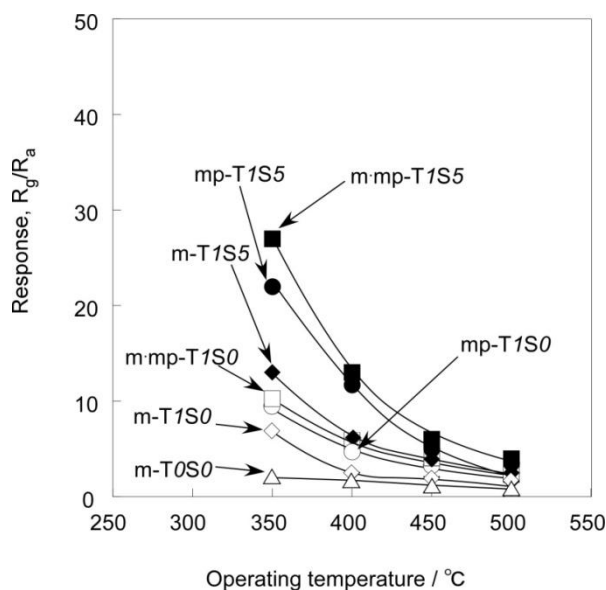


Figure 9. Temperature dependence of response SnO₂-based thick film sensors to 1 ppm NO₂.



Response transients of SnO₂-based thick film sensors to 1,000 ppm H₂ at 450 °C and 1 ppm NO₂ at 350 °C balanced with air are shown in Figures 10 and 11, respectively. In this study, 50% response time is defined as a period necessary to achieve 50% of resistance value of $R_a - R_g$, while 50% recovery time is defined as that necessary to achieve 50% of resistance value of $R_g - R_a$ for H₂.

The 50% response and recovery times to NO_2 are also defined in the similar manner, but by using $R_g - R_a$ for response time and $R_a - R_g$ for recovery time. Hereafter, they are simply expressed as response time and recovery time, respectively. Response and recovery times of SnO_2 -based thick film sensors to 1,000 ppm H_2 at 450 °C and 1 ppm NO_2 at 350 °C were summarized in Table 3. The m-T0S0 sensor showed the longest response and recovery times to H_2 among the sensors listed in Table 3. The simultaneous addition of 1 wt% SiO_2 and 5 wt% Sb_2O_5 to m-T0S0 was found to shorten slightly response and recovery times to H_2 (see m-T1S5).

Figure 10. Response transients of SnO_2 -based thick film sensors to 1,000 ppm H_2 in air at 450 °C.

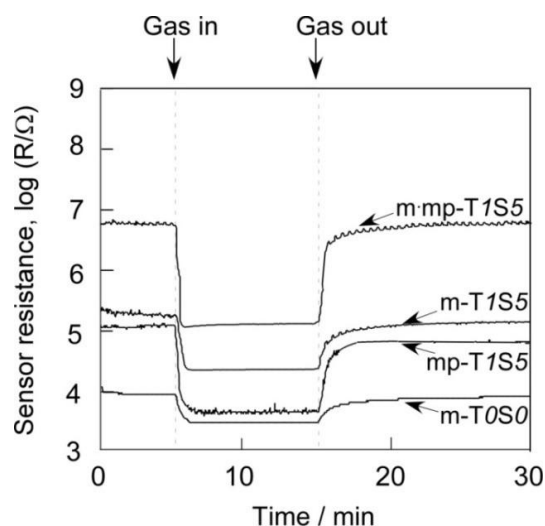
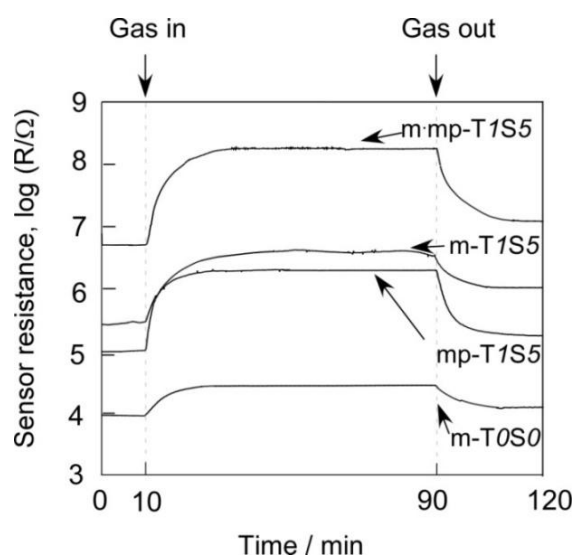


Figure 11. Response transients of SnO_2 -based thick film sensors to 1 ppm NO_2 in air at 350 °C.



However, the m-T1S5 sensor showed longer response and recovery times to 1 ppm NO_2 than m-T0S0. Thus, the effect of additive on the response and recovery times varied with the kind of target gas. The introduction of macropores into m-T1S5 shortens the response and recovery times to H_2 . More remarkable shortening of the recovery time to H_2 as well as response and recovery times to NO_2 were observed with m-mp-T1S5. It is reasonable to consider that the response time to H_2 is closely

related to the diffusivity of H_2 , while the recovery time is controlled by the diffusivity of O_2 which has a larger molecular size than H_2 . As for NO_2 , on the other hand, both the response and recovery times are considered to be affected by the diffusivity of NO_2 itself, which has a larger molecular size than H_2 , from its gas sensing mechanism. Such considerations predict a shorter recovery time to H_2 as well as shorter response and recovery times to NO_2 by the introduction of macropores into the sensor materials. The results obtained with m mp-T/S5 were in good agreement with this prediction. Thus, the mp-T/S5 sensor, which was fabricated only by the introduction of macropores, showed the fastest response to H_2 as well as the fastest response and recovery times to NO_2 among the sensors tested. But, the reason for the longer recovery time to H_2 of mp-T/S5 than m mp-T/S5 is not clear at present. Anyway, such behavior undoubtedly arises from more easy diffusion of a target gas as well as oxygen through mesopores rather than macropores. On the other hand, all of the response and recovery times to NO_2 are much longer than those to H_2 . This may arise not only from slow diffusivity of NO_2 in comparison to H_2 , but also from slow adsorption rate and strong interaction of NO_2^- species on the oxide surface.

Table 3. 50% response time and 50% recovery time of SnO_2 -based thick film sensors to 1,000 ppm H_2 at 450 °C and 1 ppm NO_2 at 350 °C balanced with air.

Sensors		1,000 ppm H_2 (450 °C)		1 ppm NO_2 (350 °C)	
Kind of powder	Abbreviation	50% response time/s	50% recovery time/s	50% response time/s	50% recovery time/s
m- SnO_2	m-T/S0	25	35	182	330
	m-T/S5	22	29	195	600
m mp- SnO_2	m mp-T/S5	20	17	154	325
mp- SnO_2	mp-T/S5	16	22	110	220

Figures 12 and 13 show variations in responses of SnO_2 -based sensors to 1,000 ppm H_2 at 450 °C and to 1 ppm NO_2 at 350 °C in air with amounts of Sb_2O_5 added, respectively. From these figures, it is also apparent that the m-T/S0 sensor showed the smallest responses to both H_2 and NO_2 among the sensors studied. The addition of 1 wt% SiO_2 to m-T/S0 enhanced responses to both H_2 and NO_2 to a certain level for every series of sensors. In addition, H_2 and NO_2 responses increased with increasing amounts of Sb_2O_5 additive in each series of sensors. On the whole, the magnitude of the response was in the order of m mp-T/Sy > mp-T/Sy > m-T/Sy, when the comparison was made at the same additive amount of Sb_2O_5 , with only one exception observed for the NO_2 response of the m mp-T/S0 sensor. It is worth noting that the mp-T/Sy series sensors showed higher H_2 and NO_2 responses than those of m-T/Sy series sensors, irrespective of their smaller surface area. This implies that all the surface of sensor materials including the inner surface of mesopores is not utilized effectively for gas detection, and that easy diffusion of a target gas as well as oxygen to the active surface, *i.e.*, the existence of certain amounts of macropores inside the thick film sensors, is more important for improving gas response. The highest H_2 and NO_2 responses observed with the m mp-T/Sy sensors may be a result of good combination of mesopore and macropores in the thick film sensors. From these results, it was revealed that the strict control of microstructure having well-developed mesoporous and macroporous

is indispensable to enhancing gas reactivity and diffusivity and thus to improving responses to H_2 and NO_2 in air.

Figure 12. Variations in response of SnO_2 -based sensors to 1,000 ppm H_2 in air at 450 °C with amounts of Sb_2O_5 added.

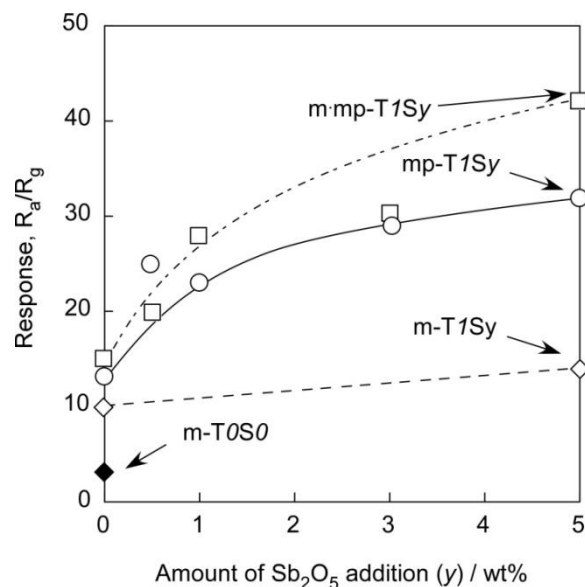
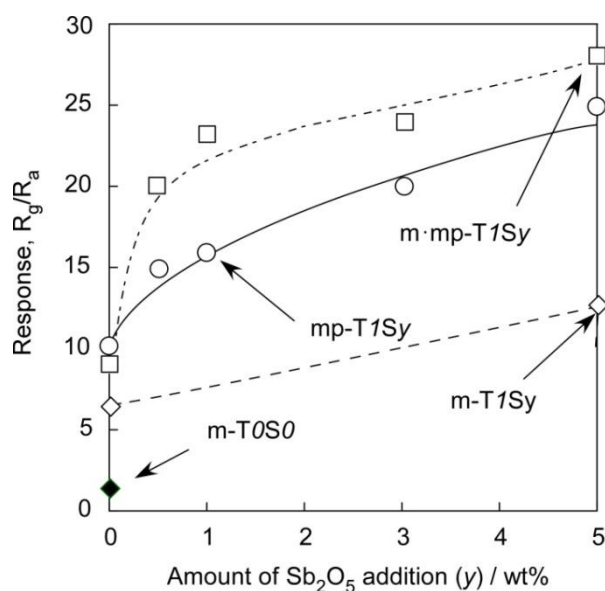


Figure 13. Variations in response of SnO_2 -based sensors to 1 ppm NO_2 in air at 350 °C with amounts of Sb_2O_5 added.



4. Conclusions

Mesoporous and/or macroporous SnO_2 -based powders have been prepared by a sol-gel method by employing $SnCl_4 \cdot 5H_2O$, ATO as a mesopore template, PMMA microspheres as a macropore template, and their gas-sensing properties as thick film sensors towards 1 ppm NO_2 as well as 1,000 ppm H_2 in air have been investigated. The addition of SiO_2 into mesoporous and/or macroporous SnO_2 was found to increase SSA of mesoporous SnO_2 . However, the SSA of all samples increased and their CS tended

to decrease slightly with the addition of the Sb_2O_5 . The additions of SiO_2 and Sb_2O_5 into mesoporous and/or macroporous SnO_2 were found to improve the sensing properties of the resulting sensors. The addition of SiO_2 into mesoporous and/or macroporous SnO_2 was found to increase the sensor resistance in air. However, the doping of Sb_2O_5 into mesoporous and/or macroporous SnO_2 was found to markedly reduce the sensor resistance in air, and to increase the response to 1,000 ppm H_2 as well as 1 ppm NO_2 in air. Among all the sensors tested, meso-macroporous SnO_2 mixed with 1 wt% SiO_2 and 5 wt% Sb_2O_5 , which were prepared with above two templates simultaneously, exhibited the largest H_2 and NO_2 responses.

References and Notes

1. Soler-Illia, G.J.A.A.; Sanchez, C.; Lebeau, B.; Patarin, J. Chemical strategies to design textured materials: From microporous and mesoporous oxides to nano networks and hierarchical structures. *Chem. Rev.* **2002**, *102*, 4093-4138.
2. Havancsak, K. Materials science: Testing and informatics I. *Mater. Sci. Forum* **2003**, *85*, 414-415.
3. Wolf, E.L. *Nanophysics and Nanotechnology: An Introduction to Modern Concepts in Nanoscience*; John Wiley & Sons: New York, NY, USA, 2004.
4. Yamazoe, N. New approaches for improving semiconductor gas sensors. *Sens. Actuat. B* **1991**, *5*, 7-19.
5. Borisenko, V.E.; Ossicini, S. *What is What in the Nanoworld: A Handbook on Nanoscience and Nanotechnology*; John Wiley & Sons: New York, NY, USA, 2004.
6. Szostak, R. *Handbook of Molecular Sieves*; Van Nostrand Reinhold: New York, NY, USA, 1992.
7. Nguyen, S.V.; Szabo, V.; Trong On, D.; Kaliaguine, S. Mesoporous silica supported LaCoO_3 perovskites as catalysts for methane oxidation. *Microporous Mesoporous Mater.* **2002**, *54*, 51-61.
8. Umbarkar, S.B.; Kotbagi, T.V.; Biradar, A.V.; Pasricha, R.; Chanale, J.; Dongare, M.K.; Mamede, A.S.; Lancelot, C.; Payen, E. Acetalization of glycerol using mesoporous $\text{MoO}_3/\text{SiO}_2$ solid acid catalyst. *J. Mol. Catal. A Chem.* **2009**, *310*, 150-158.
9. Zhong, S.H.; Li, C.F.; Li, Q.; Xiao, X.F.; Supported mesoporous SiO_2 membrane synthesized by sol-gel-template technology. *Sep. Purif. Technol.* **2003**, *32*, 17-22.
10. Li, J.; Zhang, Y.; Hao, Y.; Zhao, J.; Sun, X.; Wang, L. Synthesis of ordered mesoporous silica membrane on inorganic hollow fiber. *J. Colloid Interface Sci.* **2008**, *326*, 439-444.
11. Liu, J.; Cai, Y.; Deng, Y.H.; Sun, Z.K.; Gu, D.; Tu, B.; Zhao, D. Magnetic 3-D ordered macroporous silica templated from binary colloidal crystals and its application for effective removal of microcystin. *Microporous Mesoporous Mater.* **2010**, *130*, 26-31.
12. Fukuoka, A.; Araki, H.; Sakamoto, Y.; Inagaki, S.; Fukushima, Y.; Ichikawa, M. Palladium nanowires and nanoparticles in mesoporous silica templates. *Inorg. Chim. Acta* **2003**, *350*, 371-378.
13. Choe, Y.S. New gas sensing mechanism for SnO_2 thin-film gas sensors fabricated by using dual ion beam sputtering. *Sens. Actuat. B* **2001**, *77*, 200-208.
14. Kim, D.; Yoon, J.; Park H.; Kim, K. CO_2 -sensing characteristics of SnO_2 thick film by coating lanthanum oxide. *Sens. Actuat. B* **2000**, *62*, 61-66.

15. Hyodo, T.; Shimizu, Y.; Egashira, M. Design of mesoporous oxides as semiconductor gas sensor materials. *Electrochemistry* **2003**, *71*, 387-392.
16. Hyodo, T.; Nishida, N.; Shimizu, Y.; Egashira, M. Preparation and gas-sensing properties of thermally stable mesoporous SnO₂. *Sens. Actuat. B* **2002**, *83*, 209-215.
17. Sasahara, K.; Hyodo, T.; Shimizu, Y.; Egashira, M. Macroporous and nanosized ceramic films prepared by modified sol-gel method with PMMA microsphere templates. *J. Eur. Ceram. Soc.* **2004**, *24*, 1961-1967.
18. Hyodo, T.; Sasahara, K.; Shimizu, Y.; Egashira, M. Preparation of macroporous SnO₂ films using PMMA microspheres and their sensing properties to NO_x and H₂. *Sens. Actuat. B* **2005**, *106*, 580-590.
19. Yuan, L.; Hyodo, T.; Shimizu, Y.; Egashira, M. Preparation of mesoporous and meso-macroporous SnO₂ powders and their application to H₂ gas sensor. *Sens. Mater.* **2009**, *21*, 241-250.
20. Supothina, S. Gas sensing properties of nanocrystalline SnO₂ thin films prepared by liquid flow deposition. *Sens. Actuat. B* **2003**, *93*, 526-530.
21. Firooz, A.A.; Hyodo, T.; Mahjoub, A.R.; Khodadadi, A.A.; Shimizu, Y.; Egashira, M. Synthesis and gas-sensing properties of nano- and meso-porous MoO₃-doped SnO₂. *Sens. Actuat. B* **2010**, *147*, 554-560.
22. Hyodo, T.; Abe, S.; Shimizu, Y.; Egashira, M. Gas-sensing properties of ordered mesoporous SnO₂ and effects of coatings thereof. *Sens. Actuat. B* **2003**, *93*, 590-600.
23. Szczuko, D.; Werner, J.; Oswald, S.; Behr, G.; Wetzig, K. Surface-related investigations to characterize different preparation techniques of Sb-doped SnO₂ powders. *Appl. Surf. Sci.* **2001**, *79*, 484-491.
24. Horrillo, M.C.; Serventi, A.; Rickerby, D.; Gutierrez, J. Influence of tin oxide microstructure on the sensitivity to redactor gases. *Sens. Actuat. B* **1999**, *58*, 474-477.
25. Jones, A.; Jones, T.A.; Mann, B.; Firth, J.G. The effect of the physical form of the oxide on the conductivity changes produced by CH₄, CO and H₂O on ZnO. *Sens. Actuat.* **1984**, *5*, 75-88.
26. Xu, C.N.; Tamaki, J.; Miura, N.; Yamazoe, N. Grain size effects on gas sensitivity of porous SnO₂-based elements. *Sens. Actuat. B* **1991**, *3*, 147-155.
27. Ahn, J.P.; Kim, S.H.; Park, J.K.; Huh, M.Y. Effect of orthorhombic phase on hydrogen gas sensing property of thick film sensors fabricated by nanophase tin dioxide. *Sens. Actuat. B* **2003**, *7106*, 1-7.
28. Clifford, P.K.; Tuma, D.T. Characteristics of semiconductor gas sensors. II. Transient response to temperature change. *Sens. Actuat.* **1982**, *3*, 255-265.
29. Yamazoe, N.; Sakai, G.; Shimanoe, K. Oxide semiconductor gas sensors. *Catal. Surv. Asia* **2003**, *7*, 63-75.
30. Ahna, J.P.; Kim, J.H.; Park, J.K.; Huh, M.Y. Microstructure and gas-sensing properties of thick film sensor using nanophase SnO₂ powder. *Sens. Actuat. B* **2004**, *99*, 18-24.
31. Williams, G.; Coles, G.S.V. Gas-sensing potential of nanocrystalline tin dioxide produced by a laser ablation technique. *MRS Bull.* **1999**, *24*, 25-29.
32. Tholen, A.R. Formation and observation of ultrafine particles. *Mater. Sci. Eng.* **1993**, *A168*, 131-135.

33. Herrmann, J.M.; Disdier, J.; Fernandez, A.; Jimenez, V.M.; Sanchez-Lopez, J.C. Oxygen gas sensing behavior of nanocrystalline tin oxide prepared by the gas phase condensation method. *Nano Struct. Mater.* **1997**, *6*, 675-686.
34. Li, G.J.; Kawi, S. High-surface area SnO₂: A novel semiconductor oxide gas sensor. *Mater. Lett.* **1998**, *34*, 99-102.
35. Shimizu, Y.; Hyodo, T.; Egashira, M. Mesoporous semiconducting oxides for gas sensor application. *J. Eur. Ceram. Soc.* **2004**, *34*, 1389-1398.
36. Hieda, K.; Hyodo, T.; Shimizu, Y.; Egashira, M. Preparation of porous tin dioxide powder by ultrasonic spray pyrolysis and their application to sensor materials. *Sens. Actuat. B* **2008**, *133*, 144-150.
37. Hyodo, T.; Baba, Y.; Wada, K.; Shimizu, Y.; Egashira, M. Hydrogen sensing properties of SnO₂ varistors loaded with SiO₂ by surface chemical modification with diethoxydimethylsilane. *Sens. Actuat. B* **2000**, *64*, 175-181.
38. Li, L.L.; Mao, L.; Duan, X.C. Solvothermal synthesis and characterization of Sb-doped SnO₂ nanoparticles used as transparent conductive films. *Mater. Res. Bull.* **2006**, *41*, 541-546.
39. Wang, Y.D.; Chen, T. Nonaqueous and template-free synthesis of Sb doped SnO₂ microspheres and their application to lithium-ion battery anode. *Electrochim. Acta* **2009**, *54*, 3510-3515.
40. Kong, J.; Deng, H.; Yang, P.; Chu, J. Properties of pure and antimony-doped tin dioxide thin films fabricated by sol-gel technique on silicon wafer. *Mater. Chem. Phys.* **2009**, *114*, 854-859.

© 2011 by the authors; licensee MDPI, Basel, Switzerland. This article is an open access article distributed under the terms and conditions of the Creative Commons Attribution license (<http://creativecommons.org/licenses/by/3.0/>).